

1 **Three-way Calibration Checks Using Ground-Based, Ship-Based  
2 and Spaceborne Radars**

3 Alain Protat<sup>1</sup>, Valentin Louf<sup>1</sup>, Joshua Soderholm<sup>1</sup>, Jordan Brook<sup>2</sup>, William Ponsonby<sup>3</sup>

4 <sup>1</sup> Australian Bureau of Meteorology, Melbourne, Australia

5 <sup>2</sup> University of Queensland, Brisbane, Australia

6 <sup>3</sup> Engineering and Technology Program, CSIRO National Collections and Marine Infrastructure, Hobart, Australia

7 *Correspondence to:* Alain Protat (alain.protat@bom.gov.au)

8 **Abstract.**

9 This study uses ship-based weather radar observations collected from *Research Vessel Investigator* to evaluate the  
10 Australian weather radar network calibration monitoring technique that uses spaceborne radar observations from the  
11 NASA Global Precipitation Mission (GPM). Quantitative operational applications such as rainfall and hail  
12 nowcasting require a calibration accuracy of  $\pm 1$  dB for radars of the Australian network covering capital cities.  
13 Seven ground-based radars along the western coast of Australia and the ship-based OceanPOL radar are first  
14 calibrated independently using GPM radar overpasses over a 3-month period. The calibration difference between the  
15 OceanPOL radar (used as a moving reference for the second step of the study) and each of the 7 operational radars is  
16 then estimated using collocated, gridded, radar observations to quantify the accuracy of the GPM technique. For all  
17 seven radars the calibration difference with the ship radar lies within  $\pm 0.5$  dB, therefore fulfilling the 1 dB  
18 requirement. This result validates the concept of using the GPM spaceborne radar observations to calibrate national  
19 weather radar networks (provided that the spaceborne radar maintains a high calibration accuracy). The analysis of  
20 the day-to-day and hourly variability of calibration differences between the OceanPOL and Darwin (Berrimah)  
21 radars also demonstrates that quantitative comparisons of gridded radar observations can accurately track daily and  
22 hourly calibration differences between pairs of operational radars with overlapping coverage (daily and hourly  
23 standard deviations of  $\sim 0.3$  dB and  $\sim 1$  dB, respectively).

**Deleted:** evaluate

24 **1 Introduction**

25 Operational radar networks play a major role in providing situational awareness and nowcasting in severe  
26 weather situations, including heavy rain, flash floods, hailstorms, and wind gusts. Such radar-based information is  
27 then used by forecasters as guidance for issuing severe weather warnings. The quality of these radar-derived  
28 products in real-time is driven to a large extent by how well the underlying radar measurements are calibrated.  
29 Recently, the Australian Bureau of Meteorology (BoM) has developed an operational radar calibration framework to  
30 monitor the calibration of all BoM operational radars in real-time (Louf et al. 2019, hereafter L19). This approach is  
31 based on a combination of three techniques. The objective of this technique is to achieve an absolute calibration  
32 accuracy better than 1 dB, which is the operational calibration requirement in Australia for quantitative use of the  
33 Australian weather radar observations over capital cities (so-called Tier 1 radars). At the heart of this framework lies  
34 the so-called Volume Matching Method (VMM), initially developed by Schwaller and Morris (2011) and further

**Deleted:** and pointing accuracy

**Deleted:** As will be described in more detail later, t

**Deleted:** , allowing

**Deleted:** for an

40 improved by Warren et al. (2018, hereafter W18). In this VMM technique, intersections between individual ground-  
41 based radar beams and NASA Tropical Rainfall Measurement Mission (TRMM, Simpson et al. 1996) or Global  
42 Precipitation Mission (GPM, Hou et al. 2014) scanning Ku-band radar beams are averaged over an optimally  
43 defined common sampling volume (see W18 for more detail). In what follows, we will use the term "calibration" to  
44 refer to calibration differences between ground or ship-based radars and the GPM radar taken as the "reference".  
45 However, it must be noted that reflectivities measured by the GPM radar are not a normed reference, which implies  
46 that our use of the term "calibration" is strictly not correct.

47 A major advantage of using the GPM VMM technique is that the spaceborne radar provides a single source  
48 of reference to calibrate all radars of an operational network. Despite multiple possible sources of errors contributing  
49 to the VMM calibration error estimate, such as temporal mismatch, imperfect attenuation corrections, gridding and  
50 range effects, and differences in radar minimum detectable signal, the overall accuracy of such technique is thought  
51 to be better than 2 dB for individual overpasses (Schwaller and Morris, 2011; W18; L19, It must be noted however  
52 that there has been no independent quantification of this accuracy. This is the main objective of this study, where we  
53 use dual-polarization C-band weather radar (OceanPOL) observations collected on board the Marine National  
54 Facility (MNF) Research Vessel (RV) Investigator between Darwin and Perth, Australia, as part of the *Years of the*  
55 *Maritime Continent – Australia* (YMCA, Protat et al. 2020) and the *Optimizing Radar Calibration and Attenuation*  
56 *corrections* (ORCA) experiments to evaluate the approach of calibrating a whole radar network using GPM. The  
57 concept of this study is presented in Fig. 1. GPM observations are first used to calibrate both the ship-based radar  
58 and all the operational ground-based radars along the western coast of Australia independently. The ship-based radar  
59 observations calibrated using GPM are then individually compared with those from each ground-based radar as the  
60 ship sails close to them. Since all radars (including OceanPOL) have been calibrated using GPM, the differences  
61 between ship-based and ground-based observations can be interpreted as an error estimate of the GPM calibration  
62 technique, with some unknown additional contribution from errors due to the ship-ground radar comparisons  
63 themselves. These errors coming from ship-ground comparisons are expected to be much lower than those arising  
64 from the GPM / ground radar comparisons. Indeed, the advantage of using a ship-based radar relative to a  
65 spaceborne radar is that many of the error sources in ground-based / satellite radar comparisons are reduced to a  
66 minimum. Taking advantage of a month-long dataset of calibration difference estimates between OceanPOL and the  
67 Darwin radar, we also assess the operational potential of daily and calibration change monitoring using overlapping  
68 ground-based radar observations.

69 The remainder of this paper is organized as follows. In section 2, we briefly describe the YMCA and  
70 ORCA experiments, the characteristics of radars used in this study, and the calibration techniques. In section 3, we  
71 present the main findings of this study. Concluding remarks are presented in section 4.

## 72 2 Radar observations during YMCA and ORCA and calibration comparisons

73 In this section, we briefly introduce the datasets collected during the YMCA and ORCA experiments, the  
74 details of all radars involved in this study, and the techniques used to calibrate the ground and ship radars with the  
75 spaceborne radar and to compare ground and ship radars.

76 **Deleted:** ), but

**Deleted:** The

**Deleted:** like OceanPOL

**Deleted:** the GPM

**Deleted:** , allowing for an upper bound for the natural variability of  
radar calibration to be estimated, as will be discussed later...

## 2.1 The YMCA and ORCA experiments

84 *RV Investigator* OceanPOL radar observations used in this study were collected as part of two back-to-back  
 85 field experiments. The first experiment is the Australian contribution to the Years of the Maritime Continent  
 86 (YMCA), which is an international coordinated effort to better understand the organization of coastally induced  
 87 convection over the Maritime Continent and its complex interactions with large-scale drivers, with the ambition to  
 88 better represent these processes in global circulation models characterized by large and persistent rainfall biases.  
 89 During the second phase of YMCA (12 November – 19 December 2019), the sampling strategy was to position *RV*  
 90 *Investigator* off the coast around Darwin in a dual-Doppler configuration with either the Warruwi (north-east of  
 91 Darwin) or Berrimah (Darwin) operational C-band Doppler radars to characterize the rainfall, morphological, and  
 92 dynamical properties of convective systems developing near the coast and propagating offshore, which are  
 93 particularly poorly forecasted in this region (e.g., Neale and Slingo, 2002; Nguyen et al. 2017a,b), but are thought to  
 94 contribute about half of the rainfall along tropical coasts (e.g., Bergemann et al. 2015). In this study, we also take  
 95 advantage of the month-long time series of OceanPOL – Berrimah radar observations to quantify the variability of  
 96 radar calibration on daily and hourly timescales.

97 The second field experiment (ORCA) was conducted during a transit voyage to relocate *RV Investigator*  
 98 from Darwin to Perth, Western Australia. This transit voyage was an ideal opportunity to collect collocated radar  
 99 samples with several operational radars along the coast (Fig. 1). Specific stops of three hours were scheduled in the  
 100 vicinity of each radar in the event of precipitation within range of OceanPOL and of the ground-based radar. Of the  
 101 eight possible radars, we have luckily been able to collect such collocated precipitation samples for six of them,  
 102 except Geraldton and Carnarvon. In this study we will use all these collocated samples to quantify how well the  
 103 calibration estimate provided for each radar by the GPM technique agree with the calibration estimates obtained  
 104 using OceanPOL as a second and more accurate source of reference.

## 105 2.2 The radars ~~of~~ this study

106 Table 1 summarizes the relevant information about all radars used in this study. ~~The Australian radar~~  
 107 network comprises a large variety of radars from different generations, frequencies (although radars in this study are  
 108 all C-band radars, ~~other parts of the country are covered by S-band radars~~, beamwidths (ranging from 1.0° to 1.7°),  
 109 range resolutions (ranging from 250m to 1000m), and total time to complete ~~each~~ volumetric sampling (from 6 min  
 110 for more recent radars to 10 minutes for older radars). At the time of the YMCA and ORCA experiments, all radars  
 111 operated continuously. The Berrimah (Darwin) and Serpentine (Perth) radars are Tier 1 radars (as they cover capital  
 112 cities), while all other radars in Table 1 are Tier 2 radars. Tier 1 and 2 radars have a calibration accuracy  
 113 requirement of better than 1 and 2 dB, respectively. ~~The internal calibration accuracy of these operational radars is~~  
 114 ~~checked six-monthly by BoM radar engineers as part of their routine maintenance. The calibration check only~~  
 115 ~~includes measurements of gains and losses at different check points of the transmission and reception chains. No~~  
 116 ~~end-to-end calibration using external targets is ever performed. Special visits to sites are organized when a radar is~~  
 117 ~~down or when complaints are issued by the public about radar data quality.~~

118 The GPM KuPR and OceanPOL radars are the most modern radars. It must be noted that the OceanPOL  
 119 radar is the only dual-polarization radar. This important feature for several applications is not used in the present  
 120 study, except for the quality control of the OceanPOL radar data. ~~A critical aspect of operating a radar on a research~~

**Deleted:** involved in

**Deleted:** As clearly illustrated from this table,

**Deleted:** but

**Deleted:** the

125 vessel is the need to compensate for ship motions and velocity in real-time. To do so, the OceanPOL antenna control  
126 system ingests the real-time inertial motion unit data from the ship at 10 Hz and steers the radar beam in real-time in  
127 the requested azimuth and elevation direction. The accuracy of this stabilization has been found to produce a  
128 pointing accuracy better than 0.1°, even in harsh sea conditions. Doppler measurements are automatically corrected  
129 in real-time for the Doppler component induced by ship velocity components. Dual-polarization moments are also  
130 corrected using the statistical corrections proposed in Thurai et al. (2014). The same calibration procedure as that  
131 employed by BoM is used for OceanPOL (internal measurements of gains and losses, no end-to-end calibration).

132 As discussed previously, the GPM Ku-band radar measurements are considered as the reference for the  
133 calibration of all radars in this study. The GPM radar calibration procedure, described in detail in Masaki et al.  
134 (2020) inherited from years of calibration work undertaken as part of the previous satellite radar mission, the  
135 Tropical Rainfall Measurement Mission (TRMM). This calibration comprises an internal calibration (monitoring  
136 closely the gains and losses of each component of the radar) and an external calibration procedure using a ground-  
137 based calibrator and sea surface of well-known backscatter. Importantly, the GPM mission also benefits from  
138 extensive field experiments undertaken as part of the Ground Validation program, including in-situ ground and  
139 aircraft validation of the products of the GPM mission. By comparing different approaches for the GPM Ku-band  
140 radar calibration, Masaki et al. (2020) demonstrated that the accuracy of the radar was well within the ±1 dB  
141 requirement. In our study, Version 5 of the GPM 2AKu product has been used for all comparisons in this study  
142 (Kidd et al. 2017), which includes the latest calibration from Masaki et al. (2020) and contains attenuation-corrected  
143 Ku-band reflectivities. GPM attenuation correction is achieved using a hybrid approach combining the traditional  
144 Hitschfeld - Bordan technique (Hitschfeld and Bordan, 1954) and the so-called Surface Reference Technique  
145 (Meneghini et al., 2004). To compare GPM Ku-band radar with C-band radars in this study, all GPM Ku-band  
146 reflectivities have been converted to their equivalent C-band reflectivities using Eq. 5 in L19.

### 147 2.3 The S<sup>3</sup>CAR radar calibration framework

148 Recently, BoM has developed the operational S<sup>3</sup>CAR (Satellite, Sun, Self-consistent, Clutter calibration  
149 Approach for Radars) framework to monitor the calibration of the BoM operational radars in real-time (operational  
150 version of L19). This approach is based on a combination of three techniques. The first technique, the Relative  
151 Calibration Adjustment (RCA, e.g., L19; Wolff et al. 2015), assumes that the 95<sup>th</sup> percentile of "ground clutter"  
152 radar reflectivities (buildings, topographic structures, trees, etc ...) within 10 km range is constant. This technique  
153 tracks changes in daily calibration to better than 0.2 dB (L19) but does not provide an estimate of the absolute  
154 calibration. The second technique (W18) statistically compares collocated ground radar and spaceborne Ku-band  
155 radar from the NASA TRMM (1997-2014) and GPM (2014-present) missions. The operational implementation of  
156 the GPM calibration technique closely follows the description given in W18. Satellite and ground-based radar  
157 observations are first matched to a common volume. We require at least a minimum of 10 satellite profiles within  
158 the ground radar domain to select and process a satellite overpass. The melting layer is detected by the operational  
159 GPM algorithms and excluded from the matched volumes due to uncertainties in frequency conversions for melting  
160 hydrometeors. Matched volumes in both liquid and ice phases are retained (like in W18). Non-uniform beam filling  
161 effects of the matched volumes are mitigated by only selecting volumes that are 95% filled. A maximum ground-  
162 based reflectivity threshold of 36 dBZ is used in the analysis of matched volumes to mitigate the potential impact of  
163 attenuation correction errors.

Formatted: Superscript

Deleted: The dark art of radar calibration

Deleted: , whose calibration is very accurately tracked by NASA

166 From our experience, and as reported in L19, this technique provides an absolute calibration with an  
167 accuracy of about 2 dB from each overpass. The S<sup>3</sup>CAR framework uses the RCA technique to detect stable periods  
168 of calibration and averages calibration estimates from all GPM overpasses within each period, improving the  
169 absolute calibration accuracy, hopefully to better than 1 dB. Note that these values of 2 dB and 1 dB are qualitative  
170 error estimates based on visual inspection of the variability of calibration error estimates from successive satellite  
171 overpasses. The third technique used in S<sup>3</sup>CAR is the solar calibration technique, which is a faithful implementation  
172 of the Altube et al. (2015) method, with additional corrections for a possible levelling error of the radars as  
173 described in Curtis et al. (2021). The solar calibration technique uses sun power measurements collected at the  
174 Learmonth observatory, Western Australia. This technique is mostly used in conjunction with the RCA and GPM  
175 outputs to diagnose whether a change in calibration is due to the transmitting chain (RCA and GPM detect a change

**Deleted:** of

176 but not the solar calibration technique) or the receiving chain (all techniques detect a change). This is an important  
177 diagnostic to help radar engineers troubleshoot a radar issue and enable rapid return to service.

178 Among all operational radars considered in this study, only two of these radars (Berrimah and Geraldton)  
179 send the unprocessed reflectivities to Head Office in real-time, allowing for the full S<sup>3</sup>CAR process to be used to  
180 calibrate these radars. The term "unprocessed" here refers to radar data still containing noise and all typical radar  
181 signal contaminations, including ground clutter and sun spikes used in our calibration techniques. For the other  
182 radars, post-processing is done on-site to reduce the bandwidth required to send the radar data in real-time (these  
183 radars are in very remote places). As a result, ground clutter and sun interference have largely been removed for  
184 these radars, which implies that only the GPM part of the S<sup>3</sup>CAR framework can be used. As explained, this reduces  
185 the accuracy of the calibration estimate for such radars.

**Deleted:** raw

#### 186 2.4 Statistical comparisons between OceanPOL and the ground radars

187 Calibration between ground-based radars and OceanPOL proceeds by first gridding observations from each  
188 radar to a common 1 km horizontal / 500 m vertical resolution domain, then building a joint frequency histogram of  
189 reflectivity values from all common grid points. The expectation from such plots is that they should exhibit a  
190 systematic shift, corresponding to a difference in calibration between the two radars, with a large amount of  
191 variability in these comparisons owing to all the sources of errors involved in such comparisons (differences in exact  
192 time of observations of a grid, imperfect attenuation corrections, gridding artefacts, differences in implicit resolution  
193 of radar volumes at different ranges, differences in minimum detectable signal ...). The gridding technique used for  
194 all radars is the same and follows Dahl et al. (2019). This gridding technique uses a constant radius of influence  
195 (3.5km) and a weighted summation with distance to the centre of the grid for points belonging to the same elevation  
196 angle but a linear interpolation in the vertical using data from the elevations below and above each grid. This

**Deleted:** between

**Deleted:** elevation angles in the vertical

**Deleted:** great

197 technique has the advantage of not producing the typical artificial vertical spreading of observations below / above  
198 the lowest / highest elevation angles observed when using a radius of influence in all directions. Depending on how  
199 old the ground radars are, different minimum reflectivity thresholds are used in the comparisons to mitigate potential  
200 artefacts in calibration difference estimates due to the degraded sensitivity and reflectivity resolution of the older  
201 radars for low to intermediate reflectivities. In general, a relatively high threshold of 20-25 dBZ was required, which  
202 also had the advantage of reducing the potential impact of different non-uniform grid filling at the edges of the  
203 convective systems due to different radar detection capabilities.

209 OceanPOL data have been corrected for attenuation using the Gu et al. (2011) C-band dual-polarization  
210 technique available in the Py-ART toolkit (Helmus and Collis, 2016). The operational radars have been corrected for  
211 attenuation using C-band reflectivity – attenuation relationships derived from the OceanRAIN dataset (Protat et al.  
212 2019). It must be noted that additional comparisons done without attenuation corrections of the ground radars did  
213 not yield large differences (less than 0.5 dB in all sensitivity tests conducted). This is presumably due to the fact that  
214 there are many more points below 30-35 dBZ than above in those comparisons, resulting in a relatively minor  
215 impact of attenuation on these statistical comparisons. Also, the ship and ground radars were generally not far away  
216 from each other (typically 20-40 km), so the viewing geometry of the storms was quite similar from both radars in  
217 most cases, resulting in similar levels of attenuation along the two different paths through the storms.

218 The scanning sequence employed for OceanPOL uses the exact same 14 elevation angles used throughout  
219 the operational radar network. The start of each OceanPOL scanning sequence is synchronized with that of the  
220 operational radars running a 6-minute sequence (starts on the hour then every 6 minutes), which implies that  
221 temporal differences in volumes sampled by OceanPOL and the radars running the 6-minutes sequence are minimal.  
222 The impact of temporal evolution on the comparisons between OceanPOL and the radars running a 10-minute  
223 sequence will naturally be larger. To minimize this impact in our comparisons, we have discarded files for which the  
224 start time differs from the OceanPOL start time by more than 2 min.

225 Finally, to mitigate the potential impact of wet radome attenuation at C-band on the comparisons, we have  
226 screened out observations where precipitation was present within 5km of either of the radars from the comparisons.  
227 More precisely, for each volumetric scan we estimate the precipitation fraction within 5 km, and if more than 20%  
228 of this area is covered with precipitation, we conservatively discard this scan. However, it must be noted that results  
229 obtained when changing that threshold were very similar, with maximum statistical differences in estimated  
230 calibration difference less than 0.3 dB (not shown). From a visual inspection of radar scans, we inferred that this was  
231 due to rainfall generally not observed over and around the radars when such comparisons were made.

### 232 3 Results

233 In this section, we present the main results of this three-way calibration comparison exercise. [Comparisons](#)  
234 [between OceanPOL and the ground-based radars, all calibrated using GPM, are used to quantify the accuracy of the](#)  
235 [GPM VMM technique. The day-to-day variability of ground – ship radar comparisons over a month is also used to](#)  
236 [quantify the accuracy of daily calibration monitoring using overlapping ground-based radars and its potential for](#)  
237 [operational use. Lastly, we explore the potential for tracking calibration differences at the hourly time scale rather](#)  
238 [than the daily time scale using overlapping ground-based radars.](#)

#### 239 [3.1 The accuracy of the GPM VMM technique](#)

Formatted: Font: Bold

240 [As illustrated in Fig. 1, the first part of the calibration consistency check is to calibrate OceanPOL and the](#)  
241 [ground radars using the same single independent source, the GPM spaceborne radar. All calibration results are](#)  
242 [summarized in Fig. 2. We are fortunate enough that over two months including the YMCA and ORCA observational](#)  
243 [periods, the rainfall activity allowed us to collect a reasonable number of GPM overpasses over each radar \(except](#)  
244 [for Learmonth, radar 29, Fig. 2\). As a result, for radar 29, we will use an older calibration estimate \(-2.6 dB\),](#)  
245 [derived from a GPM overpass with many matched volumes in July 2019 and will assume that its calibration has not](#)

Deleted: .

247 changed. As discussed previously, the RCA technique can be used to accurately track changes in calibration.  
248 Unfortunately, among all radars included in Fig. 2, the RCA can only be applied to radar 63. Additional checks of  
249 the outputs of the RCA technique for radar 63 (not shown) indicated that the calibration of radar 63 had not changed  
250 over that period, which means that we can simply average all the estimates of calibration error from individual  
251 overpasses to come up with a more accurate estimate for this radar 63. Although the RCA technique cannot be used  
252 for the other radars, some insights into the calibration stability can be gained from individual calibration  
253 estimates from individual GPM overpasses in each panel of Fig. 2. Considering the expected typical error of 2 dB  
254 for individual GPM overpasses as a guideline, it seems reasonable to assume that the calibration of the OceanPOL,  
255 Warruwi (77), Dampier (15), Broome (17), and Serpentine (70) radars has not changed over the observational period  
256 either, with fluctuations around the mean calibration error estimate less than ~1.5 dB. The Port Hedland (16) radar is  
257 more problematic, as the time series shows calibration error estimates ranging from -8 dB to -2.5 dB over that  
258 period. However, the three overpass points closest to the date when collocated observations with OceanPOL were  
259 collected (26 December 2019) seem to agree reasonably well (around the mean value of -5 dB), so we will use this  
260 value of -5 dB in the following but will keep in mind the lower confidence in this calibration figure.

261 The final step of this calibration consistency check study consists in using the OceanPOL radar (previously  
262 calibrated using GPM, Fig. 2) as a second moving reference to compare with the ground-based radars. As explained  
263 earlier, satellite – ground comparisons are characterized by multiple sources of errors, including differences in  
264 sampled volumes (although great care is taken to match sampling volumes as accurately as possible, e.g., Schwaller  
265 and Morris 2011, W18, L19), non-uniform beam filling effects, temporal mismatch between observations,  
266 differences in minimum detectable signal, and radar frequency differences requiring conversion (most problematic  
267 in the melting layer and ice phase of convective storms where this correction is more uncertain, see W18). In  
268 comparison, ship radar – ground radar comparisons, especially when radars are, as in this study, reasonably close to  
269 each other to minimize differences in sampling volumes, are less prone to all these errors. The radar frequency is the  
270 same. The sampling volume and temporal mismatches are also expected to be less problematic (but not entirely  
271 negligible, especially for the radars running a 10-min sequence, see discussion in section 2.4). These more accurate  
272 ship – ground radar comparisons should therefore be considered as an indirect evaluation of the GPM validation  
273 technique and if successful, a demonstration of the value of using such GPM data as a single source of reference for  
274 the calibration of a whole national network as is done in Australia with S<sup>3</sup>CAR.

275 Figure 3 shows an example of the 2D frequency histograms of reflectivity that are used to estimate  
276 calibration differences between OceanPOL and any of the radars. This particular figure is for the Berrimah radar  
277 (63) for one day (21 November 2019) of the YMCA experiment. Such frequency distribution plots can be  
278 normalized in two different ways. If the number of points in each reflectivity pixel is divided by the total number of  
279 points (as in Fig. 3a), it highlights where most of the comparison points are in the reflectivity – reflectivity space,  
280 and therefore what contributes most to the mean calibration difference estimate. When the number of points in each  
281 pixel is divided by the total number of points in each reflectivity bin on the x-axis (Fig. 3b), the joint distribution  
282 provides a better visual sanity check of the systematic shift of the joint distribution produced by the calibration  
283 difference over the whole reflectivity range and allows detection of other potential artefacts. In the example of Fig.  
284 3a, which is typical of all comparisons made in this study, it is clear that reflectivities less than 35 dBZ contributed  
285 most to the estimation of the mean calibration difference of 0.9 dB between the two radars. On another hand, Fig.

**Deleted:**

**Deleted:** (discussed later and shown as black dots in Fig. 4)

**Deleted:** these two radars

**Deleted:** these

**Deleted:** s

**Deleted:** Looking at the time series of GPM calibration estimates for other radars than 63 and c...

**Deleted:** for

**Deleted:** In a perfect world

**Deleted:** , there should be no statistical difference between OceanPOL and the ground-based radars since they have all been calibrated using the same source of reference (GPM). However, a...

**Deleted:** typical

**Deleted:** on the left panel of

**Deleted:** right panel of

**Deleted:** it

**Deleted:** for

**Deleted:** to be detected

**Deleted:** most of the points that

**Deleted:** are clearly of reflectivity less than 35 dBZ

**Deleted:** the right panel

307 [3b](#) shows more clearly that there is indeed a consistent shift in reflectivity values across the whole reflectivity range,  
308 as expected from a (systematic) calibration difference. An important feature of Fig. 3 is the observed large  
309 variability around the mean calibration difference. The standard deviation of calibration difference for all  
310 comparisons in this study, was typically between 4 and 6 dB. It must be noted that this large standard deviation is an  
311 estimation of the errors on calibration difference of each individual pixel, not that of the daily estimate. The higher  
312 number of days spent collecting collocated observations off the Berrimah (63) and Warruwi (77) radars also offers  
313 an opportunity to estimate daily calibration differences and take a closer look at the day-to-day variability of  
314 calibration differences.▼

**Deleted:** and

**Deleted:** We will get back to that point shortly.

315 When including all days of observations for radars 63 and 77 (25 days for radar 63 and 4 days for radar 77  
316 with precipitation), the mean calibration difference between OceanPOL and radars 63 and 77 are 0.4 dB and -0.3  
317 dB, respectively (see Fig. 4 for radar 63, Fig. 5a for radar 77, see also Table 2 for a summary of all calibration  
318 differences found in this study). The [other relatively recent, better-quality operational radar included in this study](#) is  
319 radar 70 (Perth). For this radar, only short duration drizzle and scattered showers were observed when *RV*  
320 *Investigator* approached its destination (Fremantle port), resulting in less points for the calibration difference  
321 estimate. Despite the short duration dataset for radar 70, the 2D joint histogram of reflectivities show a consistent  
322 difference across the whole reflectivity range, with a mean calibration difference of -0.4 dB (Fig. 5f). These three  
323 estimates are well below the required accuracy of 1 dB for operational applications, which indicates that for these  
324 four good-quality radars (OceanPOL and radars 63, 77, and 70), the GPM comparisons provided a consistent  
325 calibration to within  $\pm 0.5$  dB. However, those are the comparisons where errors were expected to be smallest, given  
326 the large number of days included in the comparisons for radars 63, and the excellent synchronization of the 6-min  
327 scanning sequences with OceanPOL for these three radars.

**Deleted:** next best

**Deleted:**

328 Let us now turn our attention to the quantitative comparisons between OceanPOL and the older operational  
329 radars (15, 16, 17, 29) running with a 10-minute scanning sequence and / or a degraded range resolution (as reported  
330 in Table 1), and only a few opportunistic hours of collocated samples with precipitation (see list of time spans in  
331 Table 2). Visual inspection of gridded radar data revealed the presence of strong anomalous propagation (AP) signal  
332 in the lower levels (up to about 2km height ASL) for radars 15, 16, and 29, which has not been filtered correctly by  
333 the operational radar post-processing suite. This problem is well known to the BoM forecasters. As a result, for these  
334 radars, two sets of results are presented in Table 2. Calibration differences obtained from all data are labelled "AP"  
335 and those obtained when screening out all common grids below 2km height are labelled "noAP". Figure 5 shows the  
336 2D joint histograms of reflectivity when the anomalous propagation is screened out. The largest impact of  
337 anomalous propagation is found for radar 16, with a difference of 0.9 dB between estimates with and without AP  
338 screening. For the two other radars 15 and 29, the impact is modest (0.3 to 0.5 dB). This is due to the higher  
339 proportion of samples located below 2 km height for the radar 16 case (not shown) than for the two other cases.  
340 Overall, this result is shown to illustrate that particular attention needs to be paid in regions prone to anomalous  
341 propagation effects. From Table 2 and Fig. 5, the calibration differences with OceanPOL for these older radars are  
342 +0.3 dB (radar 15), +0.1 dB (radar 16), +0.4 dB (Broome, radar 17), and +0.1 dB (radar 29). In summary, all seven  
343 radars considered in these comparisons are characterized by calibration differences with OceanPOL within  $\pm 0.5$  dB,  
344 despite the large variability in radar quality and number of samples included in the calibration difference estimates  
345 (reported in Fig. 5). As a result, we can safely conclude that these comparisons validate the concept of using the

350 GPM VMM calibration technique as a single source of reference to accurately calibrate and monitor calibration of  
351 national radar networks.

**3.2 The accuracy of daily calibration monitoring from overlapping ground-based radars**

**Formatted:** Font: Bold

353 As introduced earlier, the day-to-day variability of calibration differences between ship and ground-based  
354 radars can be analysed using the month of collocated samples between OceanPOL and the Berrimah radar collected  
355 during YMCA (coloured points in Fig. 4). From Fig. 4, some simple statistics can be derived and discussed. The  
356 minimum and maximum calibration differences over the month-long time series are -0.2 and +1.1 dB, which  
357 corresponds to minimum and maximum differences of -0.6 and +0.7 dB around the mean value of 0.4 dB. The  
358 colour of the points is the number of samples that were available to estimate the daily calibration difference. The  
359 coloured error bars are estimates of the hourly standard deviation of calibration difference for each day. From a  
360 close inspection of the location of points with respect to the mean value for the period, there does not seem to be any  
361 obvious relationship between the number of points and how close the estimates are to the mean value of 0.4 dB. This  
362 result shows that the number of samples is not the main source of differences between daily estimates.

**Deleted:** , which will be discussed in more detail later

363 The standard deviation of daily calibration difference between Berrimah and OceanPOL over this month of  
364 data is 0.33 dB (Fig. 4). Since this standard deviation value includes any potential natural variability of the daily  
365 calibration difference and the variability due to uncertainties in these daily ship – ground radar comparisons such as  
366 spatial resolution differences and temporal mismatches, this value of 0.33 dB can be considered as an upper bound  
367 for the uncertainty in daily calibration difference estimates. To check whether the natural variability of daily radar  
368 calibration was minimal over that month of Darwin observations, we have added in Fig. 4 the time series of daily  
369 mean RCA values (black points) used as part of our operational S<sup>3</sup>CAR calibration monitoring technique as another  
370 calibration variability metrics. It has been shown that this RCA technique could track changes in daily calibration to  
371 better than about 0.2 dB (L19). To better compare variabilities obtained from calibration differences and the RCA,  
372 we have subtracted the mean RCA (54.11 dBZ) value to each daily RCA value and added the mean calibration  
373 difference over the whole period (0.4 dB), so that the daily RCA time series is centred on the mean calibration  
374 difference (blue line). Over this whole period, the standard deviation of the RCA value is 0.12 dB, which confirms  
375 the L19 results. This standard deviation is smaller than that of the OceanPOL – Berrimah comparisons (0.33 dB). If  
376 we assume that the standard deviation of the RCA value is an upper bound for the natural variability of the daily  
377 calibration figure, this result shows that most of the variability in calibration difference between the OceanPOL and  
378 Berrimah radars (0.33 dB) is in fact a measure of the inherent uncertainties of gridded radar comparisons. This  
379 important result highlights that such quantitative comparisons of overlapping gridded radar observations can be  
380 successfully used to monitor the consistency of daily calibration of operational radars with overlapping coverage to  
381 better than the 1 dB requirement.

**3.3 The accuracy of hourly calibration monitoring from overlapping ground-based radars**

**Formatted:** Font: Bold

383 The last thing we explore with this Darwin dataset is the potential for tracking calibration differences at the  
384 hourly time scale rather than the daily time scale. To do so, for each day of observations, we have estimated the  
385 calibration difference from 1-hour chunks of collocated data, then estimated the standard deviation of the hourly  
386 estimates for each day. An example of such daily analysis is shown in Fig. 6 for a day (08/12/2019) where 15

388 successive hours of collocated samples were available. Although this example includes more hours of comparisons  
389 than most other days, it is very typical in terms of the hour-to-hour variability we observe each day, making it a  
390 good candidate for illustrative purposes. We have not elected to screen out hours with fewer points, which, as can be  
391 seen from hours 14 and 15, would have resulted in a lower hourly standard deviation for that case. This should  
392 probably be done in an operational implementation. In this respect, the standard deviation of hourly calibration  
393 difference presented in Fig. 4 can be considered as an upper bound for the hourly standard deviation. The hourly  
394 standard deviation is shown in Fig.6 as a red error bar on top of the daily average point, and as a coloured error bar  
395 over each daily average in Fig. 4. Over the 1-month study period, the average hourly standard deviation derived  
396 from all hourly estimates is 0.8 dB, which is within the 1 dB requirement, but the two extreme values are 0.5 and 1.5  
397 dB (Fig. 4), indicating that occasionally the hourly estimates of calibration difference would not fully meet this  
398 requirement. From Fig. 4, it also appears that there is no inverse relationship between the number of samples and the  
399 hourly standard deviation, which could have perhaps been expected. For instance, the two points with highest hourly  
400 standard deviation (02 and 06 December 2019) are at both ends of the number of samples spectrum, and the three  
401 points with the lowest hourly standard deviations are in the lower half of the number of samples spectrum. Fig.4 also  
402 shows that when using the hourly standard deviation as an error bar, the mean value over that period (0.4 dB) is  
403 always included within one standard deviation of the daily estimate. These results would obviously need to be  
404 confirmed with more observations in the future but do highlight the potential for hourly tracking of calibration  
405 differences, enabling very early detection of issues with operational radars. 

**Deleted:** daily

#### 406 4 Conclusions

407 In this study, we have used collocated observations between spaceborne, ship-based, and ground-based  
408 radars collected during the YMCA (off Darwin) and ORCA (transit voyage between Darwin and Perth) experiments  
409 to gain further insights into the suitability and accuracy of using spaceborne radar observations from the GPM  
410 satellite mission to calibrate national operational radar networks, and to assess the potential of using data from  
411 overlapping ground-based radars to track calibration changes operationally at the daily and hourly time scales.

412 A major advantage of the GPM VMM technique is that all radars of the network are calibrated against a  
413 single source of reference. The GPM VMM literature (Schwaller and Morris, 2011; W18; L19), suggests that errors  
414 are of about 2 dB from individual GPM overpasses to better than 1 dB when stable periods of calibration can be  
415 estimated using the RCA technique and individual GPM estimates can be averaged. However, these errors have  
416 never been fully quantified. Using collocated weather radar observations between the OceanPOL radar on RV  
417 Investigator and 7 operational radars off the northern and western coasts of Australia (all calibrated using GPM), we  
418 found that for all seven operational radars, the calibration difference with OceanPOL was within  $\pm 0.5$  dB, well  
419 within the 1 dB requirement for quantitative radar applications (-0.3, +0.4, +0.4, +0.1, +0.3, +0.1, and -0.4 dB). This  
420 important result validates the concept of using the GPM spaceborne radar observations to calibrate national weather  
421 radar networks.

422 From the longer YMCA dataset collected when RV Investigator was stationed off the coast of Darwin for  
423 about a month, the day-to-day variability of calibration differences between the OceanPOL and Darwin (Berrimah)  
424 radars was estimated and compared with the daily calibration variability estimated using the RCA technique. From  
425 these comparisons, we found that the natural variability of daily radar calibration was small over our month of  
426 observations ( $\sim 0.1$  dB daily standard deviation). These comparisons also demonstrated that the intercomparison of

**Deleted:** ¶

**Deleted:** using a single source of reference

**Deleted:** in the same way

**Deleted:** Error

**Deleted:** estimates in the

**Deleted:** hint at

**Deleted:** a value

**Deleted:** ¶

**Deleted:** have

437 gridded radar observations had the potential to estimate calibration differences between radars with overlapping  
438 coverage to within about 0.3 dB at daily time scale and about 1 dB at hourly time scale. Such technique will be  
439 added to our operational S<sup>3</sup>CAR calibration monitoring framework as an additional calibration monitoring reference  
440 between GPM overpasses when the RCA technique cannot be applied.

441 **Acknowledgments**

442 The Authors wish to thank the CSIRO Marine National Facility (MNF) for its support in the form of *RV Investigator*  
443 sea time allocation on Research Voyages IN2019\_V06 (YMCA) and IN2019\_T03 (ORCA), support personnel,  
444 scientific equipment, and data management. Tom Kane and Mark Curtis from BoM are also warmly thanked for  
445 always patiently answering our relentless questions about the Australian weather radar network intricacies.  
446

447 **Code availability**

448 Codes developed for this study are protected intellectual property of the Bureau of Meteorology and are not publicly  
449 available.  
450

451 **Data availability**

452 All OceanPOL and Level 1b data from the operational radar network used in this study are available at  
453 <http://www.openradar.io>. The NASA GPM radar data were obtained using the STORM online data access interface  
454 to NASA's precipitation processing system archive (<https://storm.pps.eosdis.nasa.gov>).  
455

456 **Sample availability**

457 No samples were used in this study.  
458

459 **Author contribution**

460 AP, JS, VL, JB, and WP collected the datasets used in this study. VL produced the GPM comparisons using the  
461 operational S3CAR technique. JS produced post-processed volumetric and gridded data for all ground-based radars.  
462 VL produced the gridded OceanPOL data. JB developed the gridding technique used in this study. AP designed and  
463 coordinated the YMCA and ORCA field experiments, analyzed the results, and wrote the manuscript. VL, JS, JB,  
464 and WP provided edits of the manuscript.  
465

466 **Competing interests:**

467 The authors declare that they have no conflict of interest.  
468

469 **References**

470 Altube, P., J. Bech, O. Argemi, and T. Rigo: Quality control of antenna alignment and receiver calibration using the  
471 sun: Adaptation to midrange weather radar observations at low elevation angles. *J. Atmos. and Ocean. Technol.*,  
472 32, 927-942, 2015.  
473 Bergemann, M. M., C. Jakob, and T. P. Lane: Global detection and analysis of coastline-associated rainfall using an  
474 objective pattern recognition technique. *Journal of Climate*. 28, 18, p. 7225-7236, 2015.  
475

**Deleted:** , <https://doi.org/10.1175/JTECH-D-14-00116.1>

475 Curtis, M., G. Dance, V. Louf, and A. Protat: Diagnosis of Tilted Weather Radars Using Solar Interference. *J.  
476 Atmos. Oceanic Tech.*, 38, 1613-1620, 2021. Deleted: in Press, June

477 Dahl, N. A., A. Shapiro, C. K. Potvin, A. Theisen, J. G. Gebauer, A. D. Schenkman, and M. Xue: High-Resolution,  
478 Rapid-Scan Dual-Doppler Retrievals of Vertical Velocity in a Simulated Supercell. *J. Atmos. and Ocean.  
479 Technol.*, 36, 1477-1500, 2019. Deleted: DOI: 10.1175/JTECH-D-18-0211.1

480 Gu, J.-Y., A. Ryzhkov, P. Zhang, P. Neilley, M. Knight, B. Wolf, and D.-I. Lee: Polarimetric Attenuation  
481 Correction in Heavy Rain at C Band. *Journal of Applied Meteorology and Climatology*, 50(1), 39-58, 2011. Deleted: <https://doi.org/10.1175/2010JAMC2258.1>

482 Helmus, J. J., and S. M. Collis.: The Python ARM Radar Toolkit (Py-ART), a Library for Working with Weather  
483 Radar Data in the Python Programming Language. *Journal of Open Research Software*, 4(1), e25, 2016. Deleted: <https://doi.org/10.5334/jors.119>

484 Hitschfeld, W., and J. Bordan: Errors inherent in the radar measurement of rainfall at attenuating wavelengths.  
485 *J. Meteor.*, 11, 58-67, 1954. Deleted: [https://doi.org/10.1175/1520-0469\(1954\)011.0058:EITRM.2.0.CO;2...](https://doi.org/10.1175/1520-0469(1954)011.0058:EITRM.2.0.CO;2...)

486 Hou, A. Y., and Coauthors: The Global Precipitation Measurement mission. *Bull. Amer. Meteor. Soc.*, 95, 701-722,  
487 2014. Deleted: <https://doi.org/10.1175/BAMS-D-13-00164.1>

488 Kidd, C., J. Tan, P.-E. Kirstetter, and W. A. Petersen: Validation of the Version 05 Level 2 precipitation products  
489 from the GPM core observatory and constellation satellite sensors. *Q J R Meteorol Soc.*, 144, 313-328. Deleted: English (Australia)

490 Louf, V., A. Protat, C. Jakob, R. A. Warren, S. Rauniar, W. A. Petersen, D. B. Wolff, and S. Collis: An integrated  
491 approach to weather radar calibration and monitoring using ground clutter and satellite comparisons. *J. Atmos.  
492 Oceanic Tech.*, 36, 17-39, 2019. (L19)

493 Masaki, T., T. Iguchi, K. Kanemura, K. Furukawa, N. Yoshida, T. Kubota, and R. Oki: Calibration of the Dual-  
494 Frequency Precipitation Radar Onboard the Global Precipitation Measurement Core Observatory. *IEEE  
495 TRANSACTIONS ON GEOSCIENCE AND REMOTE SENSING*, 2020. Deleted: https://doi.org/10.1175/JTECH1664.1,

496 Meneghini, R., J. Jones, T. Iguchi, K. Okamoto, and J. Kwiatkowski: A hybrid surface reference technique and its  
497 application to the TRMM precipitation radar. *J. Atmos. Oceanic Technol.*, 21, 1645-1658, 2004. Deleted: DOI:10.1002/qj.3168,

498 Neale, R., and J. Slingo: The maritime continent and its role in the global climate: A GCM study. *J. Clim.*, 16, 834-  
499 848, 2002. Deleted: DOI:10.1002/qj.3056,

500 Nguyen, H., C. Franklin, and A. Protat: Understanding model errors over the Maritime Continent using CloudSat  
501 and CALIPSO simulators. *Quart. J. Roy. Meteor. Soc.*, 2017. Deleted: <https://doi.org/10.1002/qj.3609-2020>,

502 Nguyen, H., A. Protat, L. Rikus, H. Zhu and M. Whimpey: Sensitivity of the ACCESS forecast model statistical  
503 rainfall properties to resolution. *Quart. J. Roy. Meteor. Soc.*, 2017. Deleted: [https://doi.org/10.1029/2019JD031011,](https://doi.org/10.1029/2019JD031011)

504 Protat, A. and I. McRobert: Three-dimensional wind profiles using a stabilized shipborne cloud radar in wind  
505 profiler mode. *Atmos. Meas. Tech.*, 13, 3609-3620, 2020. Deleted: [https://doi.org/10.1175/2010JTECHA1403.1,](https://doi.org/10.1175/2010JTECHA1403.1)

506 Protat, A., C. Klepp, V. Louf, W. Petersen, S. P. Alexander, A. Barros, and G. G. Mace: The latitudinal variability  
507 of oceanic rainfall properties and its implication for satellite retrievals. Part 2: The Relationships between Radar  
508 Observables and Drop Size Distribution Parameters. *J. Geophys. Res. Atmos.*, 124, 13312-13324, 2019. Deleted: [https://doi.org/10.1007/BF01029783,](https://doi.org/10.1007/BF01029783)

509 Schwaller, M. R., and K. R. Morris: A ground validation network for the Global Precipitation Measurement mission.  
510 *J. Atmos. Oceanic Technol.*, 28, 301-319, 2011. Deleted: [https://doi.org/10.1175/2010JTECH-A1403.1,](https://doi.org/10.1175/2010JTECH-A1403.1)

511 Simpson, J., C. Kummerow, W.-K. Tao, and R. F. Adler: On the Tropical Rainfall Measuring Mission (TRMM).  
512 *Meteor. Atmos. Phys.*, 60, 19-36, 1996. Deleted: [https://doi.org/10.1007/BF01029783,](https://doi.org/10.1007/BF01029783)

513 Thurai, M., P. T. May, and A. Protat: Shipborne polarimetric weather radar: Impact of ship movement on  
514 polarimetric variables. *J. Atmos. Oceanic Tech.*, 31, 1557-1563, 2014. Deleted: [https://doi.org/10.1175/2010JTECH-A1403.1,](https://doi.org/10.1175/2010JTECH-A1403.1)

529 Warren, R. A., A. Protat, V. Louf, S. T. Siems, M. J. Manton, H. A. Ramsay, and T. Kane: Calibrating ground-based  
 530 radars against TRMM and GPM. *J. Atmos. Oceanic Tech.*, 35, 323-346, 2018. (W18)

531 Wolff, D. B., D. A. Marks, and W. A. Petersen: General application of the relative calibration adjustment (RCA)  
 532 technique for monitoring and correcting radar reflectivity calibration. *J. Atmos. Oceanic Technol.*, 32, 496-506,  
 533 2015.

**Deleted:** <https://doi.org/10.1175/JTECH-D-13-00185.1>

534  
 535 **Tables**

Radar ID or Platform	Name	Make	(lat, lon)	Band	$\omega$ (°)	$\Delta r$ (m) / $\Delta t$ (min)
GPM	KuPR	N/A	Variable	Ku	0.7	125 / NA
RV Investigator	OceanPOL	DWSR-2501C-SDP	Variable	C	1.3	125 / 6
15	Dampier	WSR81C	(-20.654; 116.683)	C	1.7	1000 / 10
16	Port Hedland	TVDR2500-8	(-20.372; 118.632)	C	1.7	500 / 10
17	Broome	DWSR2502C-8	(-17.948; 122.235)	C	1.7	500 / 10
29	Learmonth	TVDR2500-8 (Digital upgrade)	(-22.103; 113.999)	C	1.7	250 / 10
63	Berrimah (Darwin)	DWSR2502C-14	(-12.456; 130.927)	C	1.0	250 / 6
70	Serpentine (Perth)	TVDR2500-14	(-32.392; 115.867)	C	1.0	500 / 6
77	Warruwi	DWSR2502C-14	(-11.648; 133.380)	C	1.0	250 / 6

536 Table 1: Main characteristics of the radars used in this study: radar ID in the operational radar network or platform,  
 537 name, make, coordinates, frequency band, beamwidth  $\omega$  (°), range bin size  $\Delta r$  (m), and total time to complete the

539 volumetric sampling  $\Delta t$  (min). OceanPOL and all ground-based radars have been manufactured by the Enterprise  
540 Electronics Corporation (EEC).

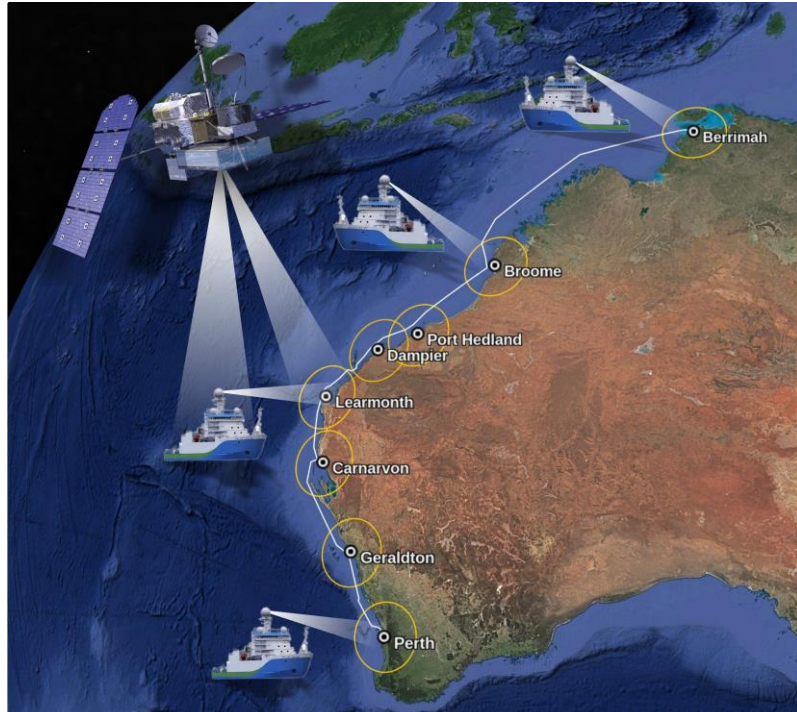
Date	Time Span (UTC)	Radar	Calibration Error (Radar – OceanPOL)
20191115	04:00 – 07:00	77	-0.2
20191117	04:00 – 08:00	77	+0.5
20191127	06:00 – 11:00	77	-0.2
20191128	03:00 – 07:00	77	-0.6
All dates above	All time spans above	77	-0.3
All dates in Fig. 4	Miscellaneous	63	+0.4
20191225	12:00 – 21:00	17	+0.4
20191226	18:00 – 24:00	16	-0.8 (AP) / +0.1 (noAP)
20191227	08:00 – 11:00	15	-0.2 (AP) / +0.3 (noAP)
20191228	08:00 – 11:00	29	-0.2 (AP) / +0.1 (noAP)
20200102	03:00 – 05:00	70	-0.4

541 Table 2: Ground radar – OceanPOL calibration difference estimates for all comparisons of this study. A mean  
542 calibration difference for radars 63 and 77 that includes all dates and time spans is also provided. For radars 15, 16,  
543 and 29, two estimates are provided, with no test on minimum height (AP) or with a minimum height of 2 km for the  
544 comparisons (noAP), in an attempt to remove residual anomalous propagation artefacts observed for these radars.

545

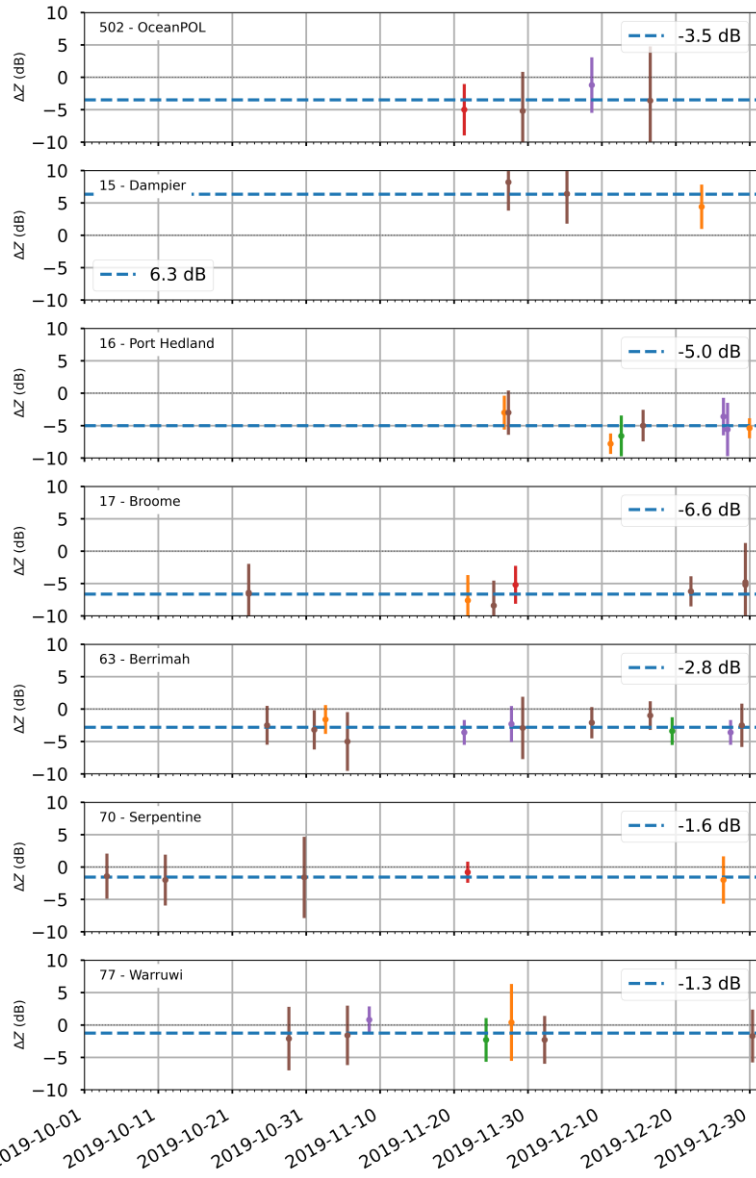
546

547 **Figures**



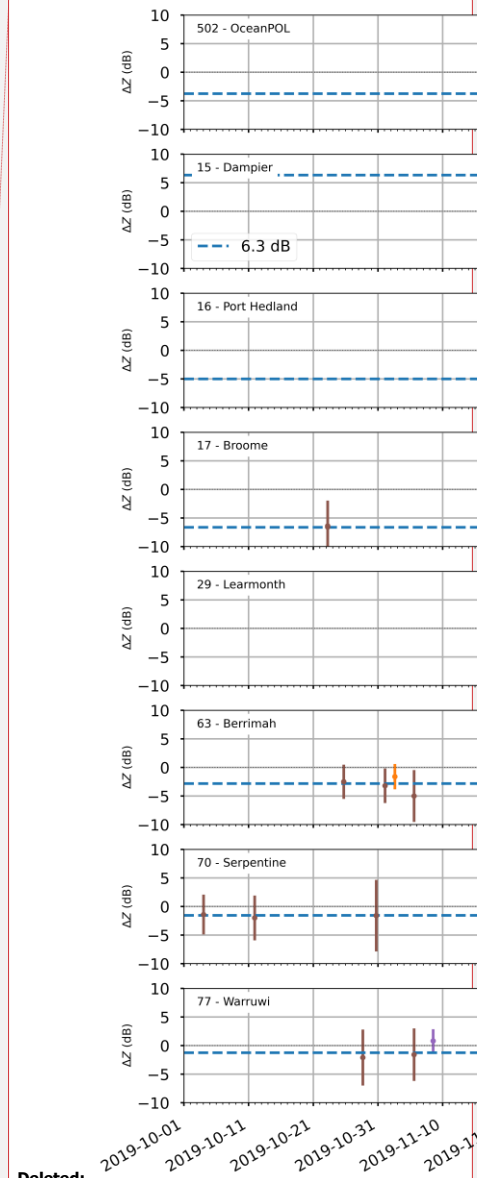
548

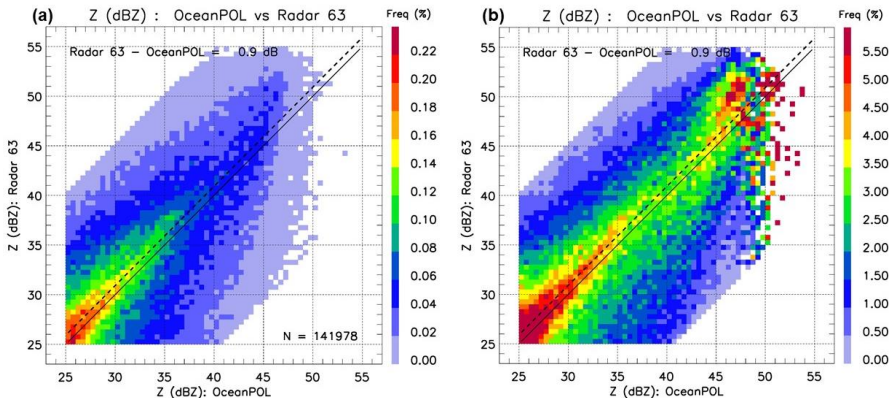
549 Figure 1: The concept of this study. Ship-based OceanPOL radar and ground-based radars are calibrated independently  
550 using the GPM Ku-band spaceborne radar, then all ground radars are compared with OceanPOL during the ORCA  
551 voyage as RV Investigator sails south. The 150 km radius of each radar is shown by a yellow circle and the ship track is  
552 shown using a white line. © 2021 Google Earth; Map Data: SIO, NOAA, U.S. Navy, NGA, GEBCO; Map Image:  
553 Landsat/Copernicus.



555  
556  
557  
558  
559  
560

Figure 2: Individual calibration error estimates from the GPM comparisons, for all radars used in this study. The standard deviation of the PDF of reflectivity difference is also shown for each estimate as an error bar. The mean value over the whole period is displayed as a dashed line for each radar, and the value is reported on the upper-right of each panel. Note that a negative value mean that the radar is under-calibrated (radar – GPM). The colour of each overpass point is the number of matched volumes: less than 20 (blue), 20 to 60 (orange), 60 to 100 (green), 100 to 150 (red), 150 to 200 (purple) or more than 250 (brown).

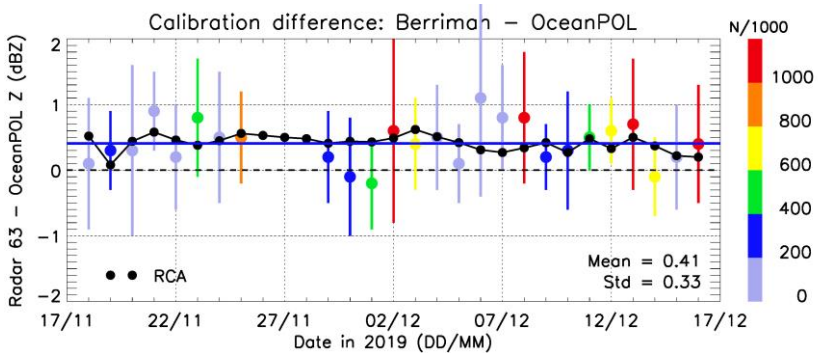




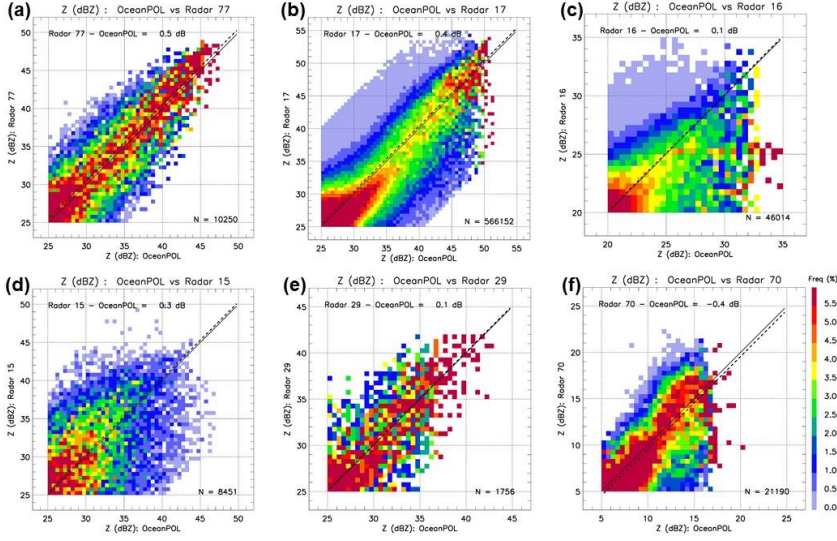
563  
564 **Figure 3:** Illustration of 2D joint frequency histograms of reflectivity used to compare quantitatively the OceanPOL radar  
565 (x-axis) and any of the ground-based radar (y-axis), [here for the Berrimah radar \(63\) for one day \(21 November 2019\) of](#)  
566 [the YMCA experiment](#). For each plot, the 1:1 line is drawn as a solid line, and the calibration difference estimate is  
567 written and shown as a dashed line. The colours show the frequency of points falling in each [reflectivity pixel 0.5 dB in](#)  
568 [resolution](#) of the 2D joint histograms, either expressed as the % of the total number of points (panel a) or as a % of the  
569 sum of points for each value of OceanPOL reflectivity (i.e., sum of all points along the y-axis at each constant value of the  
570 x-axis). [The number of samples N for this case is 141978 \(see panel a\).](#)

**Deleted:** The pixel size used for these plots is 0.5 dB.

**Deleted:** is also written in



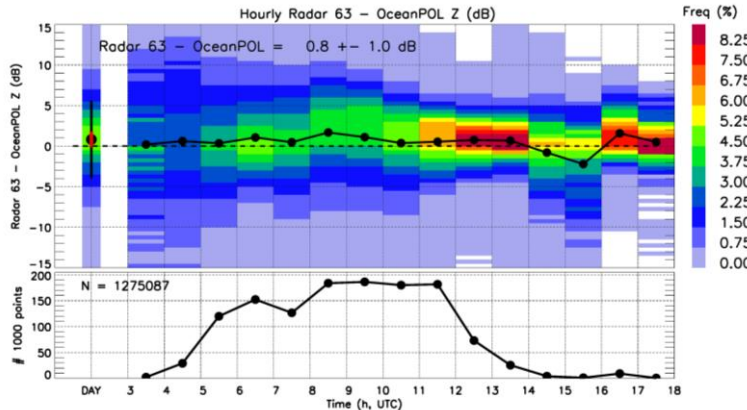
571  
572  
573 **Figure 4:** Time series of calibration differences between OceanPOL and radar 63 (Berrimah) during the YMCA  
574 experiment. Each coloured point is a daily estimate of calibration difference. The colour of the point is the number of  
575 points for each comparison, and the coloured error bar is the standard deviation of hourly calibration difference  
576 estimates for that day (see text and Fig. 6 for more details). The solid blue line is the mean value obtained from all these  
577 daily estimates (0.4 dB). The overall mean and standard deviation of the daily calibration difference over the period of  
578 observations are also written on the lower-right side of the figure. The black dashed line is the zero line. The black points  
579 are the daily outputs of the RCA values, with the mean RCA value over the period subtracted and the mean value of  
580 calibration difference added, so that the time series is centred on the mean calibration difference value.



585

586 Figure 5: 2D joint histograms of reflectivity as in Figure 3b but for radars (a) 77, (b) 17, (c) 16, (d) 15, (e) 29, and (f) 70.  
 587 Values of calibration differences are also reported in Table 2. The number of samples N is also given in each panel.

588



589

590 Figure 6: Hourly analysis of calibration differences between Berrimah (radar 63) and OceanPOL for a selected day  
 591 (08/12/2019). The upper panel shows each hourly calibration estimate as a black dot, as well as the full frequency  
 592 distribution of differences within each hour (colours). The first column of the upper-panel shows the daily summary,  
 593 including the mean value (black dot, value is also written), the frequency distribution of calibration differences (colours),  
 594 the standard deviation of the difference using the N collocated samples (black error bar), and the standard deviation of  
 595 the hourly estimates of calibration differences for that day (red error bar, value is also written). Lower panel shows the  
 596 number of samples in each hour (note y axis is the number of points divided by 1000) and the total number of samples N  
 597 is also provided.